PAPER • OPEN ACCESS

A detailed investigation of single-photon laser enabled Auger decay in neon

To cite this article: Daehyun You *et al* 2019 *New J. Phys.* **21** 113036

View the article online for updates and enhancements.

New Journal of Physics

The open access journal at the forefront of physics

PAPER

A detailed investigation of single-photon laser enabled Auger decay in neon

Daehyun You[1], Kiyoshi Ueda[1], Marco Ruberti[2], Kenichi L Ishikawa[3,4,5], Paolo Antonio Carpeggiani[6], Tamás Csizmadia[7], Lénárd Gulyás Oldal[7] , Harshitha N G[7], Giuseppe Sansone[8,9], Praveen Kumar Maroju[9], Kuno Kooser[10,15], Carlo Callegari[11] , Michele Di Fraia[11], Oksana Plekan[11], Luca Giannessi[11,12], Enrico Allaria[11], Giovanni De Ninno[11,13], Mauro Trovò[11], Laura Badano[11], Bruno Diviacco[11], David Gauthier[11], Najmeh Mirian[11], Giuseppe Penco[11] , Primož Rebernik Ribič[11], Simone Spampinati[11], Carlo Spezzani[11], Simone Di Mitri[11], Giulio Gaio[11] and Kevin C Prince[11,14]

1   Institute of Multidisciplinary Research for Advanced Materials, Tohoku University, Sendai 980-8577, Japan
2   Department of Physics, Imperial College London, London SW7 2AZ, United Kingdom
3   Department of Nuclear Engineering and Management, Graduate School of Engineering, The University of Tokyo, 7-3-1 Hongo, Bunkyo-ku, Tokyo 113-8656, Japan
4   Photon Science Center, Graduate School of Engineering, The University of Tokyo, 7-3-1 Hongo, Bunkyo-ku, Tokyo 113-8656, Japan
5   Research Institute for Photon Science and Laser Technology, The University of Tokyo, 7-3-1 Hongo, Bunkyo-ku, Tokyo 113-0033, Japan
6   Institut für Photonik, Technische Universität Wien, A-1040 Vienna, Austria
7   ELI-ALPS, ELI-HU Non-Profit Ltd., Dugonics tér 13, H-6720 Szeged, Hungary
8   ELI-ALPS, Pintér József utca, 6728 Szeged, Hungary
9   Physikalisches Institut, Universität Freiburg, D-79106 Freiburg, Germany
10 Department of Physics and Astronomy, University of Turku, Finland
11 Elettra-Sincrotrone Trieste, I-34149 Basovizza, Trieste, Italy
12 ENEA C.R. Frascati, I-00044 Frascati, Rome, Italy
13 Laboratory of Quantum Optics, University of Nova Gorica, Nova Gorica 5001, Slovenia
14 Centre for Translational Atomaterials, Swinburne University of Technology, Melbourne 3122, Australia
15 Institute of Physics, University of Tartu, EST-50411 Tartu, Estonia

E-mail: kiyoshi.ueda@tohoku.ac.jp and prince@elettra.eu

Keywords: laser enabled Auger decay, free-electron laser, neon

Abstract

Single-photon laser enabled Auger decay (spLEAD) is an electronic de-excitation process which was recently predicted and observed in Ne. We have investigated it using bichromatic phase-locked free electron laser radiation and extensive angle-resolved photoelectron measurements, supported by a detailed theoretical model. We first used separately the fundamental wavelength resonant with the Ne^+ $2s$–$2p$ transition, 46.17 nm, and its second harmonic, 23.08 nm, then their phase-locked bichromatic combination. In the latter case the phase difference between the two wavelengths was scanned, and interference effects were observed, confirming that the spLEAD process was occurring. The detailed theoretical model we developed qualitatively predicts all observations: branching ratios between the final Auger states, their amplitudes of oscillation as a function of phase, the phase lag between the oscillations of different final states, and partial cancellation of the oscillations under certain conditions.

1. Introduction

Much of experimental physics is concerned with measuring the response of matter to excitation, for example exposure to radiation. The products of this interaction may be detected; in particular, for ionisation, the ejected electrons, ions and any neutral fragments may be observed. If an ionised target such as an atom or molecule is in an excited state, then it will dispose of its excess energy by various de-excitation processes. Well known examples thereof include the emission of photons at various wavelengths: x-ray, UV–visible and infrared fluorescence, for core, electronic and vibrational excitations respectively. An important channel that is active for most core

excited atoms and molecules is Auger decay [1, 2], in which a singly ionised species decays to a doubly ionised state, with the emission of an electron which carries away (in whole or in part) the excess energy as kinetic energy.

De-excitation processes have been studied since the early part of the 20th century, so it is surprising that some have only been predicted and observed recently. An example of a recent discovery is single-photon laser enabled Auger decay (spLEAD) [3, 4]. In this process, an excited atomic or molecular ion that does not contain sufficient internal energy to decay by an Auger process is immersed in a laser field, and can obtain the missing energy by absorption of a photon from the field. The final products, a doubly charged ion and an electron, are the same as in a conventional Auger process. Laser enabled Auger decay had been observed previously for the case of multiphoton absorption from the laser field [5, 6]. However, in the multiphoton case, the dominant contributions to the cross section, within the electric dipole approximation, consist of the products of two or more single-electron dipole matrix elements between uncorrelated states, and are therefore insensitive to electron correlation. In contrast, in the case of spLEAD, the initial and final electronic configurations 'cannot be coupled by the single-electron dipole operator [...] and, as a result, the spLEAD process is forbidden in the first order similarly to the related radiative Auger process' [3]. This is what makes spLEAD of particular interest: in a first approximation (of pure electronic states) it is usually forbidden, but becomes allowed due to correlation, or configuration interaction. Thus spLEAD promises to provide insight into multielectron phenomena.

In this paper we report a detailed investigation of spLEAD in neon atoms, which we first reported in [4], using monochromatic or phase-locked bichromatic laser light. The latter is not a prerequisite for spLEAD to occur, but in the simpler case of monochromatic light it is often difficult to distinguish spLEAD from other processes, such as two-photon ionisation of an ion. It has been shown that by using phase-locked bichromatic light, interference conditions can be created such that the same final state is reached by two quantum paths [4], one of which is spLEAD. The observation of the interference then proves that the process is active, and so our experimental method provides a window for observing spLEAD.

We measure the photoelectron angular distribution (PAD) and its asymmetry A, to investigate the effect of intensity and relative phase of the two light fields on the process of interest, and we compare our results with theoretical calculations. The rest of the manuscript is structured as follows: in section 2 we introduce the necessary notation and the basic processes that may be active in the experiment; in sections 3 and 4 we describe respectively the experimental and theoretical methods used. In section 5 we present the experimental results, for the four cases of: fundamental wavelength only, second harmonic wavelength only, and phase-locked bichromatic radiation in the two limits of fundamental much weaker or much stronger than the second harmonic. In section 6 we present the theoretical results and their comparison with the experimental results, for the same four cases. In section 7 we present our summary and conclusions.

2. Notation and basic processes

The most general form of the electric field in our experiment is that of the bichromatic light:

$$E(t) = E_\omega(t) + E_{2\omega}(t) = \sqrt{I_\omega(t)} \cos\omega t + \sqrt{I_{2\omega}(t)} \cos(2\omega t - \phi), \tag{1}$$

where ω is the fundamental frequency and 2ω that of the second harmonic, $I_\omega(t)$ and $I_{2\omega}(t)$ their respective intensities, and ϕ is the phase between them. Because the pulses are long we omit an overall carrier-envelope phase. Unless otherwise stated, $\omega = 26.85$ eV, corresponding to the experimental $2s$–$2p$ resonance in Ne^+.
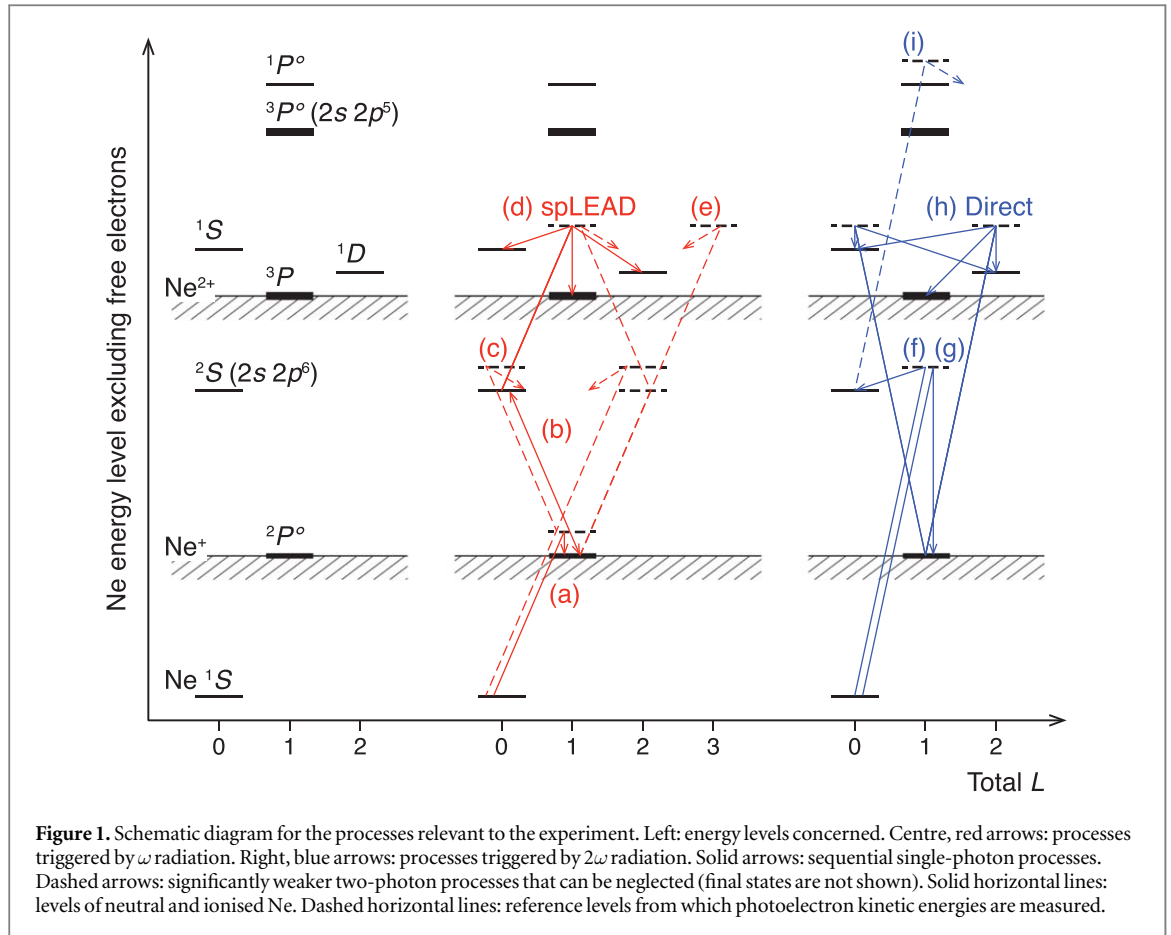
We work with spatial spherical coordinates (r, θ, φ) where θ is measured relative to the (horizontal) linear polarisation axis of the two fields, and only θ appears explicitly in the analysis of the experimental data; the asymmetry is defined for each process as the difference-over-sum of the associated photoelectron signal integrated in the two hemispheres separated by the equatorial plane:

$$A(\phi) = \frac{S_1(\phi) - S_2(\phi)}{S_1(\phi) + S_2(\phi)}, \tag{2}$$

where S_1 is the integration over the hemisphere ($0 < \theta < \pi/2$) and S_2 is the integration over the other hemisphere ($\pi/2 < \theta < \pi$). The integration procedure is obvious for the theoretical calculations, and for the experimental signal it is described in section 3. The asymmetry oscillations as a function of ϕ are modelled with a sinusoid:

$$A(\phi) = k \sin(\phi + \phi_0) + A_0, \tag{3}$$

where k is the amplitude of oscillation, ϕ_0 is the phase offset with respect to the arbitrary zero of the phase scale, and A_0 is a constant accounting for an instrumental offset related to the small spatial inhomogeneity of the detector sensitivity.

Figure 1. Schematic diagram for the processes relevant to the experiment. Left: energy levels concerned. Centre, red arrows: processes triggered by ω radiation. Right, blue arrows: processes triggered by 2ω radiation. Solid arrows: sequential single-photon processes. Dashed arrows: significantly weaker two-photon processes that can be neglected (final states are not shown). Solid horizontal lines: levels of neutral and ionised Ne. Dashed horizontal lines: reference levels from which photoelectron kinetic energies are measured.

The possible processes occurring in the experiment are listed below, and a schematic diagram is shown in figure 1. Most of these lead to singly or doubly ionised final states and the emission of an electron, but note that process (b) does not do so.

The equations governing these processes are as follows:

$$2s^2 2p^6 + \omega \rightarrow 2s^2 2p^5 + e \quad (5.19 \text{ eV or } 5.29 \text{ eV}) \tag{a}$$

$$2s^2 2p^5 + \omega \rightleftarrows 2s 2p^6 \quad \omega \text{ couples the two states} \tag{b}$$

$$2s^2 2p^6 + \omega + \omega \rightarrow 2s 2p^6 + e \quad (5.23 \text{ eV}) \tag{c}$$

$$2s 2p^6 + \omega \rightarrow 2s^2 2p^4 (^1S, {}^1D, {}^3P) + e \text{ spLEAD}$$
$$(5.88 \text{ eV}, 9.59 \text{ eV or} \sim 12.80 \text{ eV}) \tag{d}$$

$$2s^2 2p^5 + \omega + \omega \rightarrow 2s^2 2p^4 (^1S, {}^1D, {}^3P) + e \quad (5.88 \text{ eV}, 9.59 \text{ eV or} \sim 12.80 \text{ eV}) \tag{e}$$

$$2s^2 2p^6 + 2\omega \rightarrow 2s 2p^6 + e \quad (5.23 \text{ eV}) \tag{f}$$

$$2s^2 2p^6 + 2\omega \rightarrow 2s^2 2p^5 + e \quad (32.04 \text{ eV or } 32.14 \text{ eV}) \tag{g}$$

$$2s^2 2p^5 + 2\omega \rightarrow 2s^2 2p^4 (^1S, {}^1D, {}^3P) + e \quad (5.88 \text{ eV}, 9.59 \text{ eV or} \sim 12.80 \text{ eV}). \tag{h}$$

The kinetic energies of the electrons expected for $\omega = 26.85$ eV are given in parentheses in the second column; the value given for the $2s^2 2p^4 \ {}^3P$ term, 12.80 eV, is an average over the 3 levels of the multiplet [7]. Processes (a), (f) and (g) are one-photon ionisation of the ground state to give a $2p \ (^2P_{1/2}, \ ^2P_{3/2})$ or $2s$ hole state. Process (b) couples the $2s$ and $2p$ hole states, and therefore indicates both absorption and stimulated emission. Process (c) is the two-photon ionisation of the ground state to give a $2s$ hole state. This process is minor in comparison with the single ionisation process (a) to give a $2p \ (^2P_{1/2}, \ ^2P_{3/2})$ hole state or sequential two photon processes (a) and (b) to give a $2s$ hole state. Process (d) is the spLEAD process, in which a $2s$ hole state decays to a doubly ionised final state upon absorption of a photon ω. Process (e) is two-photon ionisation of the $2p$ hole state to give a doubly charged ion. This process is significantly weaker than (d). Both processes (a), (b) and (f) populate $2s$ hole states which can decay by spLEAD. Processes leading to correlation satellites, such as those from the ground state to $2s^2 2p^4 nl$, are weak and only a few series of transitions are energetically allowed: they are not considered further. For the sake of brevity, we refer hereafter to the final states of Ne^{2+} (processes (d),(e),(h)) by

their term labels alone (^1S, ^1D, ^3P), whereas 'the ion' will refer to singly-charged Ne$^+$ only, for whose states the term labels will be omitted; the $2s^2 2p^6$ ^1S ground state of neutral Ne will be referred to as 'the ground state'.

3. Experimental methods

The measurements were carried out using the velocity map imaging spectrometer (VMI) of the low density matter beamline [8] of the FERMI free electron laser [9]. The neon sample was produced using a pulsed atomic beam. The raw images acquired by the VMI were inverted using the BASEX algorithm [10]. The photoelectron spectra were generated by integrating the images in angle; the energy resolution of the VMI was 0.5 eV at 5.2 eV and 2.2 eV at 31 eV. The angular asymmetries were calculated by equation (2); in the case of bichromatic light their variation was measured as a function of phase and fitted by equation (3).

Bichromatic light at frequencies ω and 2ω was generated, and the relative phase scanned, as described in [4, 11]. The pulse durations of ω and 2ω were calculated to be 40 ± 12 fs and 30 ± 8 fs, respectively; the relative spectral bandwidth, as measured with the online spectrometer available at FERMI [12] was 1.5×10^{-3}. The spot area of the second harmonic was measured using a wavefront sensor, and was 20 μm^2, but the spot area of the fundamental wavelength could not be measured as the wavefront sensor was not sensitive at this wavelength. It is estimated to be slightly larger, based on the general properties of FERMI and of the transport optics.

The intensity at the sample was calculated from the measured pulse energies at the exit of the FERMI radiators, the measured spot area and the calculated transmission of the transport optics [13]. At 26.85 eV (ω), the theoretical transmission is 0.6, and at 53.7 eV (2ω) it is 0.77.

For bichromatic irradiation, the relative intensities of ω and 2ω can be calculated from the photoelectron intensities. The pulse energies, calculated intensity, and intensity ratios, are given in appendix. For strong ω and weak 2ω, the average intensities were 2×10^{13} and 4.6×10^{11} W cm^{-2} respectively, while for weak ω and strong 2ω, the average intensities were 6.3×10^{11} and 3×10^{13} W cm^{-2} respectively.

4. Theoretical methods

We calculated the single-atom, phase-dependent, channel-resolved asymmetry using the time-dependent (TD) B-spline algebraic diagrammatic construction (ADC) *ab initio* method [14–17]. The single-particle basis set consists of spherical harmonics $Y_{lm}(\theta, \varphi)$ for the angular part and B-spline functions $B_i(r)$ for the radial coordinate. The single particle basis functions used in this calculation are therefore expressed as:

$$\psi_{ilm} = \frac{1}{r} B_i(r) Y_{lm}(\theta, \varphi). \tag{4}$$

Due to the fact that simulation of double ionisation of Ne is too computationally demanding, the two processes consisting of the single ionisation of Ne into Ne$^+$ and the subsequent ionisation of Ne$^+$ into Ne^{2+} are described separately. Therefore, within our TD B-spline ADC approach, the 3D many-electron time-dependent Schrödinger equations (TDSE) for the neutral

$$\mathrm{i}\,\hbar\,\frac{\partial |\Psi^N(t)\rangle}{\partial t} = \hat{H}^N(t)\,|\Psi^N(t)\rangle, \tag{5}$$

and cationic system

$$\mathrm{i}\,\hbar\,\frac{\partial |\Psi^{N-1}(t)\rangle}{\partial t} = \hat{H}^{N-1}(t)\,|\Psi^{N-1}(t)\rangle, \tag{6}$$

interacting with the laser field, are solved by making the following ansatz for the TD many-electron wavefunction of neutral Ne

$$|\Psi^N(t)\rangle = \alpha_0(t)|\Psi_0^N\rangle + \sum_J \alpha_J(t)|\tilde{\Psi}_J^N\rangle, \tag{7}$$

and the Ne$^+$ ion

$$|\Psi^{N-1}(t)\rangle = \sum_I C_I(t)|\tilde{\Psi}_I^{N-1}\rangle, \tag{8}$$

respectively. Here Ψ_0^N represents the ground state of neutral Ne, while the basis functions $|\tilde{\Psi}_J^N\rangle$ and $|\tilde{\Psi}_I^{N-1}\rangle$ refer to the correlated configuration states of the ADC theory for N and $N - 1$ electrons [17, 18], respectively.

Moreover, in this work, we have used the lowest level of the ADC-hierarchy compatible with a correct description of the ionisation of Ne and Ne$^+$ by the laser pulses, i.e. ADC(1) and ADC(2)x respectively. Within ADC(1), the configuration manifold included in the description of Ne ionisation by the laser pulses, via TDSE, is the singly excited one-hole–one-particle (1h–1p) configurations. The subsequent ionisation of Ne$^+$ by the laser

pulses, which generates single excitations from the cationic states, is described, at the ADC(2)x level of theory, within the manifold of the one-hole (1h) configurations (where Ne$^+$ is described as the removal of one electron from one of the occupied orbitals in the Hartree–Fock (HF) ground state of Ne), and of the two-hole–one-particle (2h1p) configurations, where removal of one electron is accompanied by excitation of a second electron. The inclusion of the 2h1p configurations allows us to describe the doubly-ionised atom Ne^{2+} within the manifold of 2h configurations with respect to the HF state of the neutral Ne, as well as to include electron correlation in the description of the bound states of the singly-ionised Ne$^+$. With this choice, the typical number of excited configurations included in the simulation is of the order of a few tens of thousands.

During the interaction of the neutral Ne atom with the laser pulses, ionisation populates different states of the Ne$^+$ cation, namely the $2s^22p^5$ ground state, and the $2s2p^6$ state which can decay by spLEAD. Within the TD–ADC(2)x simulation of the subsequent ionisation of the Ne$^+$ cation, an initial state for the time propagation has to be chosen. This needs to model correctly the populated transient ionic state of the system. In this work, we have solved equation (6) by using as initial state both the $2s^22p^5$ Ne$^+$ state, the excited $2s2p^6$ (spLEAD active) state, as well as a complete statistical mixture of the two. Indeed, while both the $2s^22p^5$ and $2s2p^6$ ionic states are effectively populated during the ionisation of neutral Ne, the photoelectron wavepackets associated with ionisation from each of these states are characterised by different energy and/or symmetry. Therefore, the ionic system can be accurately described as a quantum-mechanically incoherent superposition of the two states [17].

The presented results have been calculated making explicit use of the atomic spherical symmetry and by describing the laser-atom interaction in length form and within the dipole approximation. The total TD Hamiltonians of equations (5) and (6) for the time-evolution of the neutral and ionic systems interacting with the ω and 2ω pulses read:

$$\hat{H}^{N/N-1}(t) = \hat{H}_0^{N/N-1} + \hat{z}E_\omega(t) + \hat{z}E_{2\omega}(t). \tag{9}$$

Here $\hat{H}_0^{N/N-1}$ are the field-free many-electron ADC(1) and ADC(2)x Hamiltonians describing the neutral (N-electron) and ionic (($N-1$)-electron) systems, respectively, and $\hat{z}$ is the dipole operator of the system along the laser-field polarisation direction. A bandwidth limited $\cos^2$ envelope was used for the pulses of both the ω and 2ω fields, with a FWHM pulse duration set to 60 fs. In this calculation we have used the estimated experimental values for the intensities of the ω and 2ω pulses. The time propagation of the unknown coefficients $\alpha_J(t)$ and $C_I(t)$ of the B-spline ADC many-electron wave-function for the neutral and ionic systems (see equations (7) and (8) respectively) is performed by means of the general complex Lanczos, or Arnoldi–Lanczos, algorithm [16, 17, 19]. The calculations have been performed using a parabolic-linear B-spline knot sequence [14, 20] with a radial box radius of $R_{\max} = 1200$ a.u. and $N_b = 1600$ radial B-splines. The maximum angular momentum employed in the expansion of equation (4) was $l_{\max} = 6$. Convergence of the results with respect to the basis set parameters has been checked.

The phase-dependent asymmetry of PADs was calculated for each possible final state $2s^22p^4(^1S)$, $2s^22p^4(^3P)$ and $2s^22p^4(^1D)$ of Ne^{2+}, by numerically integrating, at the end of the interaction with the laser pulses, in the $0 < \theta < \pi/2$ and $\pi/2 < \theta < \pi$ spatial hemispheres, the corresponding 3D ionised photoelectron wavepacket.
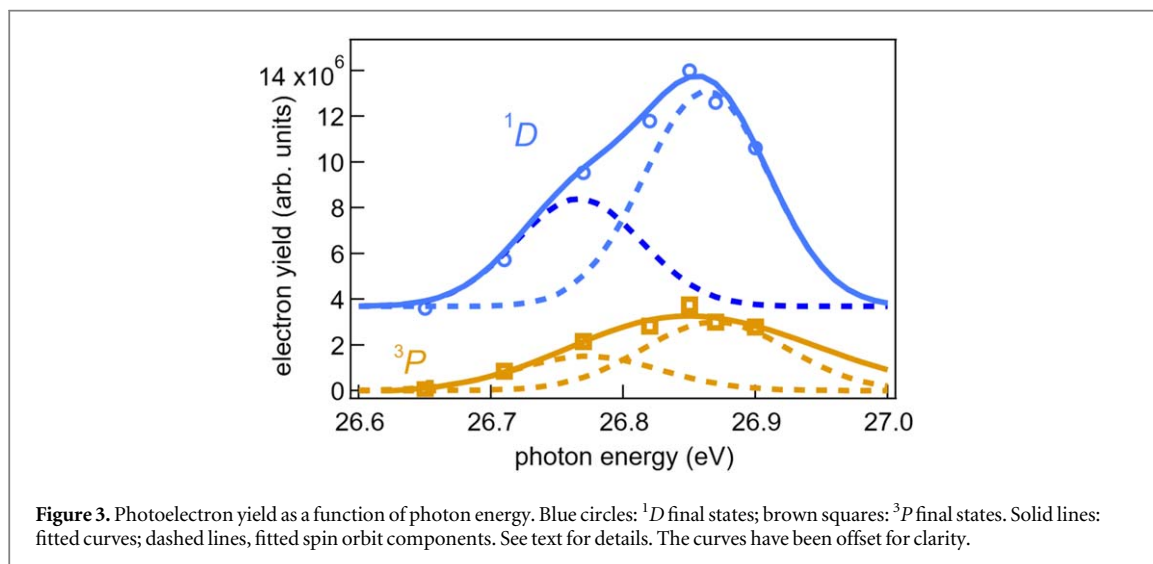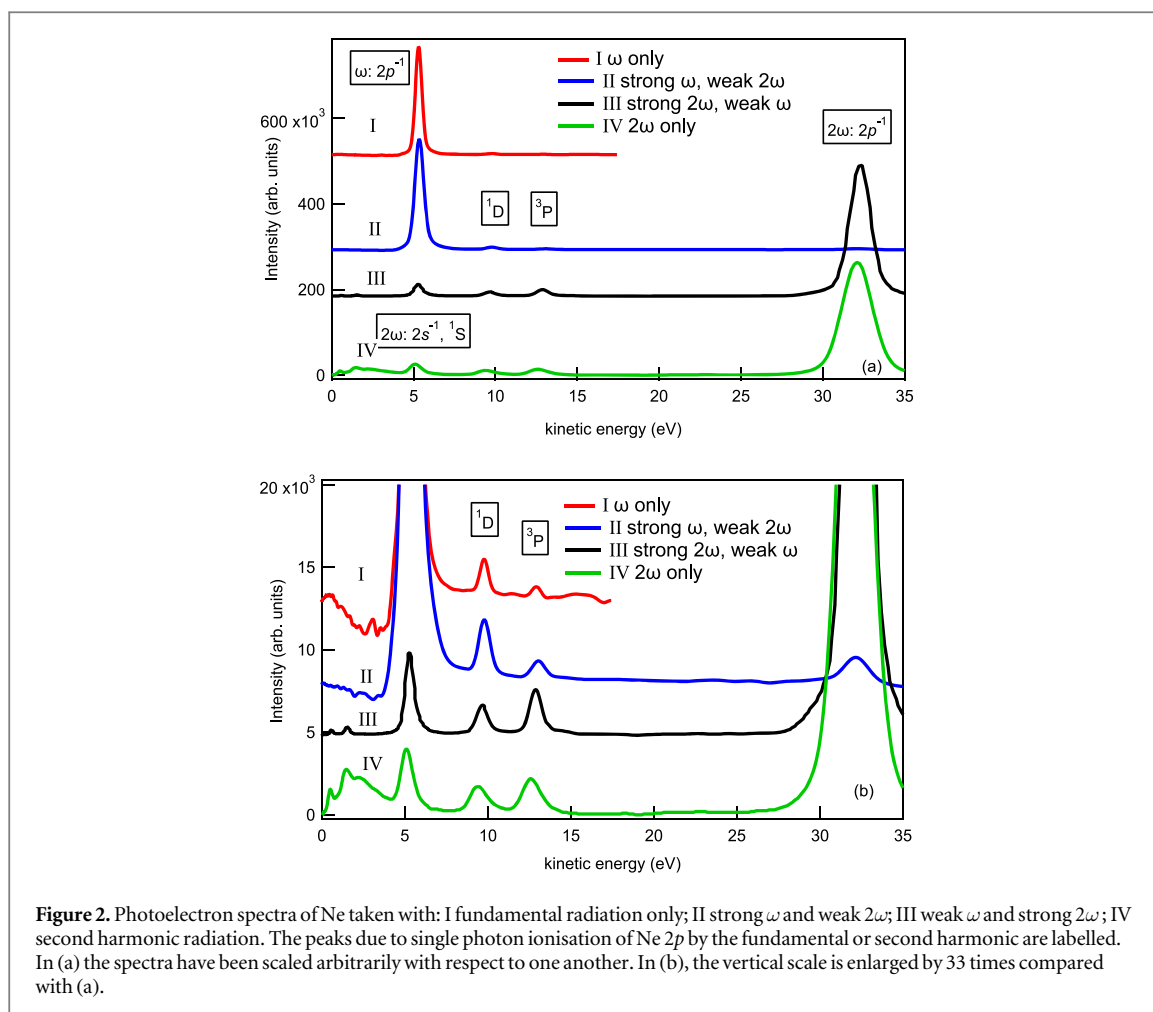
5. Experimental results

The experiments were carried out with four sets of conditions: fundamental frequency (ω) only; second harmonic frequency (2ω) only; strong ω and weak 2ω; and weak ω and strong 2ω. The photoelectron peaks are assigned based on their measured energy; when the same (or unresolved) final states correspond to more than one process, the latter are identified with the help of the calculated branching ratios of the final states, which are in general significantly different.
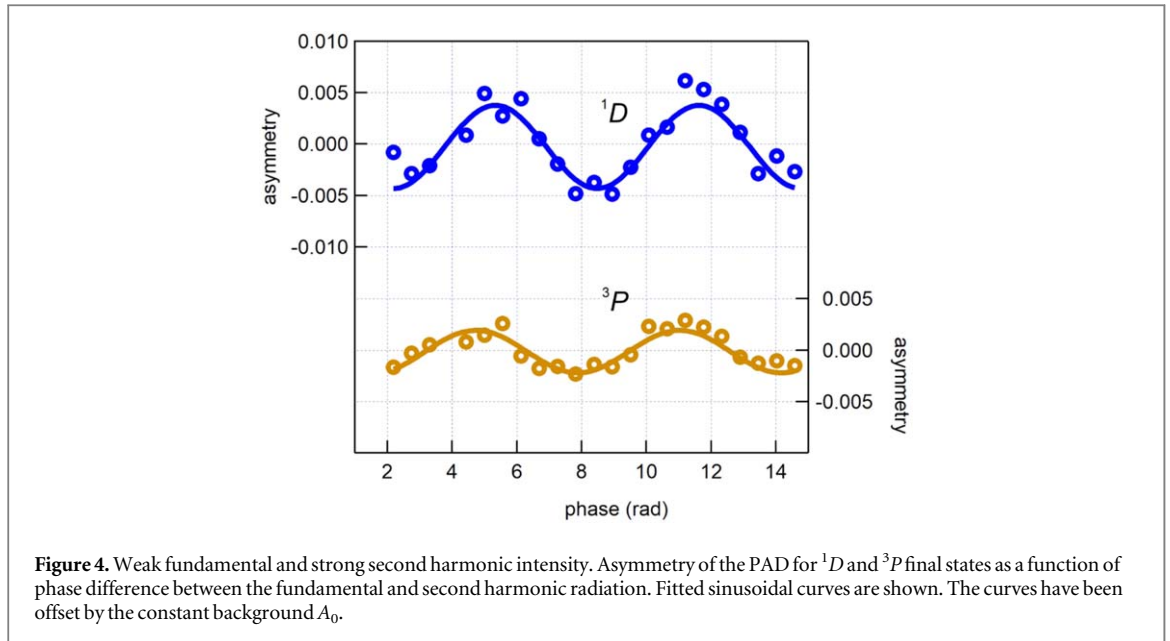
5.1. Fundamental wavelength only
In this case, only Processes (a)–(e) above are relevant. The strongest process is (a), the single-photon ionisation of the $2p$ shell of Ne. Doubly ionised final states can be reached via the sequences: (a), (b)–(d), involving spLEAD, and which is more intense; or (c), (d), (a)–(e) and (c), (b)–(e), which are significantly weaker as they involve at least one two-photon process.

Curve I in figures 2(a) and (b) show the photoelectron spectrum excited by the fundamental wavelength only, set to the resonance energy; note that the spectrum was taken over a reduced energy range of the VMI to increase energy resolution. The strongest peak at 5.19–5.29 eV and labelled 'ω: $2p^{-1}$' is assigned to process (a). Figure 2(b) reveals the photoelectrons due to the doubly ionised states, arising from paths (d) and/or (e); the ^1S state is expected at a kinetic energy of 5.95 eV [4], but is not resolved from the strong single-photon ionisation peak.

Figure 2. Photoelectron spectra of Ne taken with: I fundamental radiation only; II strong ω and weak 2ω; III weak ω and strong 2ω; IV second harmonic radiation. The peaks due to single photon ionisation of Ne $2p$ by the fundamental or second harmonic are labelled. In (a) the spectra have been scaled arbitrarily with respect to one another. In (b), the vertical scale is enlarged by 33 times compared with (a).

Figure 3. Photoelectron yield as a function of photon energy. Blue circles: ^1D final states; brown squares: ^3P final states. Solid lines: fitted curves; dashed lines, fitted spin orbit components. See text for details. The curves have been offset for clarity.

The photon wavelength was scanned to locate the resonance, or more accurately, the resonances, since the $2s^2 2p^5$ ionic state is a spin–orbit split $^2P_{1/2}$, $^2P_{3/2}$ doublet. Figure 3 shows the electron yield for the ^1D and ^3P final states as a function of photon energy. The spectra of both final states are asymmetric, due to the unresolved spin–orbit components. They were fitted with both Lorentzian and Gaussian functions which gave similar values of χ^2. Figure 3 shows Gaussian fits obtained by constraining the widths to be equal, the branching ratio to be equal to 2, and the spin–orbit separation to be 97 meV.

The resonance energy of the $^2P_{3/2}$ component was found to be 26.85 eV, within 60 meV of the expected value of 26.9104 eV [21]. The wavelength of light from FERMI is determined by that of the seed laser, whose

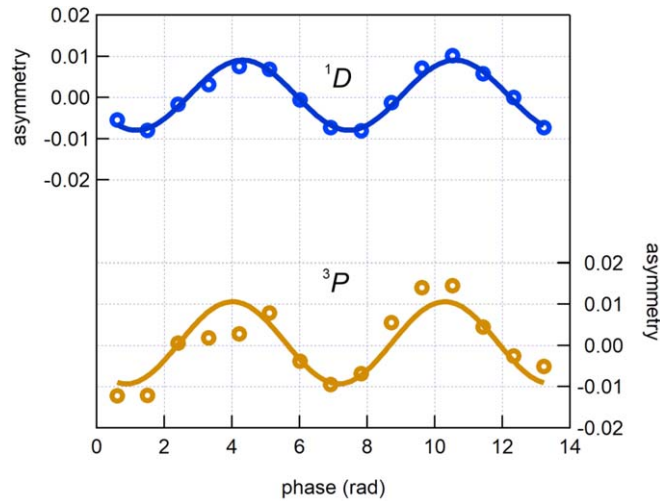**Figure 4.** Weak fundamental and strong second harmonic intensity. Asymmetry of the PAD for ^1D and ^3P final states as a function of phase difference between the fundamental and second harmonic radiation. Fitted sinusoidal curves are shown. The curves have been offset by the constant background A_0.

wavelength is measured precisely. The very small shift may be due to miscalibration or to Stark effects, so we refer to the experimental energy of 26.85 eV throughout this paper. The widths were 120 meV, significantly more than the measured spectral bandwidth of about 40 meV. This may reflect some additional jitter in the wavelength setting, or other noise. The branching ratio (ratio of areas of peaks) of ^3P relative to ^1D is 0.32.

5.2. Second harmonic wavelength only
In this case, only processes (f)–(h) above are relevant. The strongest process is (g), the single-photon ionisation of the 2*p* shell of Ne. Doubly ionised final states can be reached via the sequence: (g), (h). Curve IV in figures 2(a) and (b) shows the photoelectron spectrum excited by the second harmonic wavelength only. The strongest peak at 31 eV and labelled '2ω: $2p^{-1}$' is assigned to process (g). The peak at ∼5.2 eV is due to ionisation of the 2*s* shell of Ne, process (f); as in the case of the 2*p* ionisation by ω mentioned above, the ^1S state is expected to also be present but is unresolved. The ratio of the cross sections of process (g) over process process (f) is 21 [22], while the ratio of the experimental signals is about 17; thus the peak at ∼5.2 eV is more intense than expected on the basis of cross section, and we attribute this to a contribution from the ^1S state (process (h)). Figure 2(b), reveals the photoelectrons due to the other two doubly ionised states arising from process (h); the branching ratio of ^3P relative to ^1D is 1.07.

5.3. Bichromatic irradiation: weak fundamental intensity, strong second harmonic intensity
In this third set of measurements, we used conditions similar to those used previously [4] for a two-colour measurement. The two wavelengths are coherent and the phase ϕ was scanned to produce interference, observed as variations of the asymmetry of the PAD. A photoelectron spectrum summed over all phases is shown in figure 2 (curve III), and the asymmetry phase scan is shown in figure 4. The phase scan data were fitted with the function defined in equation (3) to extract the amplitude of the asymmetry oscillations as a function of phase, and their relative phase; the results of the fit procedure are given in table 1.

5.4. Bichromatic irradiation: strong fundamental intensity, weak second harmonic intensity
The fourth set of conditions consisted of strong fundamental intensity and weak second harmonic intensity. A spectrum summed over all phases is shown in figure 2 (curve II), and the asymmetry phase scan is shown in figure 5. The data were analysed as above, and the fit parameters are shown in table 1.

6. Analysis and discussion

6.1. Theoretical results
Figure 6 shows the configuration expansion of the 2*s* ionised eigenstate of Ne atom, calculated at the ADC(2)*x* level of theory. The main configuration (not shown in the figure) is of course $2s2p^6$ (^2S), with a coefficient $C_I^2 = 0.8$, but there are significant admixtures of other 2h1p configurations. For the case of the 2*s* ionised eigenstate, the coefficients are real, as well as of course time-independent. For the general case of a TD state the

Table 1. Parameters extracted from experimental data for the four experimental conditions, and theoretical values. $\Delta\phi_0$ is the difference in phase for the ^1D and ^3P final states determined from equation (3). BR is branching ratio.

Conditions	Final state	Parameter	Expt.	Theory
Strong ω only	—	BR ^3P:^1D	0.32	0.81
Strong 2ω only	—	BR ^3P:^1D	1.07	1.37
Weak ω, strong 2ω	^1D	k	0.0044 ± 0.0004	0.004
		A_0	0.0142 ± 0.0003	
	^3P	k	0.0021 ± 0.0001	0.003 57
		A_0	0.0047 ± 0.0002	
	—	BR ^3P:^1D	2.0	1.4
	—	k ratio ^3P:^1D	0.47 ± 0.2	0.89
	—	$\Delta\phi_0$ (rad)	-0.57 ± 0.2	-0.38
Strong ω, weak 2ω	^1D	k	0.0085 ± 0.0004	0.010 35
		A_0	0.0033 ± 0.0003	
	^3P	k	0.0100 ± 0.002	0.032
		A_0	0.034 ± 0.001	
	—	BR ^3P:^1D	0.31	0.81
	—	k ratio ^3P:^1D	1.2 ± 0.1	3.1
	—	$\Delta\phi_0$ (rad)	-0.3 ± 0.2	-1.04

Figure 5. Strong fundamental and weak second harmonic intensity. Asymmetry of the PAD for ^1D and ^3P final states as a function of phase difference between the fundamental and second harmonic radiation. Fitted sinusoidal curves are shown. The curves have been offset by the constant background A_0.
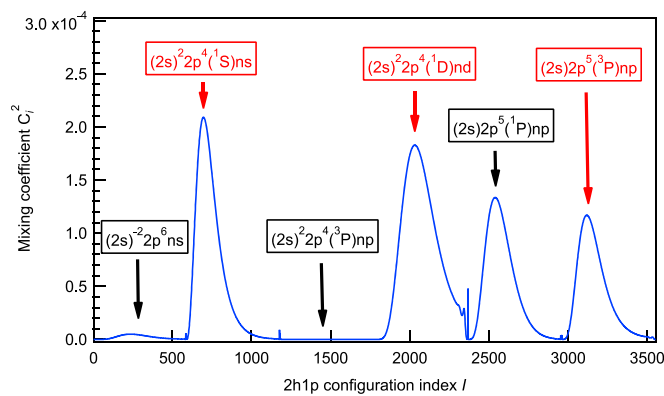

Figure 6. 2h1p configuration expansion of the $2s2p^6$ Ne$^+$ states. The *x*-axis I is the configuration index of equation (8).

Table 2. Theoretical populations for $2s2p^6$ and $2s^22p^5$ initial states. A: ω intensity $= 1.97$ $\times 10^{13}$ W cm^{-2}, 2ω intensity $= 4.6 \times 10^{11}$ W cm^{-2}. B: ω intensity $= 5.37$ $\times 10^{11}$ W cm^{-2}, 2ω intensity $= 2.79 \times 10^{13}$ W cm^{-2}. C: ω only, intensity $= 1.97$ $\times 10^{13}$ W cm^{-2}.

	Initial state	$2s^22p^4\,(^1S)$	$2s^22p^4\,(^3P)$	$2s^22p^4\,(^1D)$	BR $^3P{:}^1D$
A	$2s^22p^5$	0.000 129	0.000 506	0.000 531	0.953
A	$2s2p^6$	0.000 634	0.002 18	0.002 68	0.813
B	$2s^22p^5$	0.001 22	0.007 04	0.005 05	1.393
B	$2s2p^6$	0.000 1335	0.000 345	0.000 789	0.437
C	$2s^22p^5$	0.000 107	0.000 380	0.000 426	0.892
C	$2s2p^6$	0.002 50	0.008 00	0.009 83	0.815

coefficients of equation (8) will be both complex and TD. The configurations leading to final states with two $2p$ holes are indicated in the red boxes, and there are three, with symmetry ^1S, ^1D and ^3P, corresponding to the three doubly ionised states observed.

For the $2s^22p^4\,nl$ configurations, the spLEAD process can be thought of, in a simplified picture, as the direct ionisation of the outer nl electron, to leave the doubly ionised core. In contrast, for the $2s2p^5\,(^3P)\,nl$ configuration, $2s$–$2p$ dipole transitions with the emission of an electron give rise to spLEAD, and lead to the final $2s^22p^4\,(^3P)$ doubly ionised state.

In previous work [4], the only triplet state considered was $2s^22p^4\,(^3P)\,nl$, which as figure 6 shows, makes a negligible contribution to the configuration mixing. For this reason, it was believed that the doubly charged, triplet final state would not be populated. However the present results show that it is indeed populated, but not because of configurations built on $2s^22p^4\,(^3P)$ cores: rather, it is the configurations with $2s2p^5\,(^3P)$ cores which give rise to the doubly charged Auger triplet state.

6.2. Analysis: fundamental or second harmonic wavelength only

As noted above, the experimental branching ratio of ^3P relative to ^1D is 0.32 for the fundamental only, compared to a theoretical value of 0.81, table 1. These experimental and theoretical branching ratios are essentially the same as for the strong ω + weak 2ω case. The calculated $^3P{:}^1D$ yield ratios (0.95 for $2s^22p^5$ and 0.81 for $2s2p^6$, see table 2) are larger than the measured value of 0.32 and this might be due to a possible theoretical overestimation of the ADC(2)ext calculated transition dipoles to the ^3P dication states.

Other possible reasons for the theoretical overestimation are the simplified representation of the dication states, described within ADC(2)ext as simple double hole states, small differences between the calculated ADC (2)ext and the exact weight of the different 2h1p configurations in the expansion of the spLEAD active state, as well as to the contribution of other transiently-populated bound states of Ne$^+$ whose exact excitation energy is overestimated in the ADC(2)ext theoretical description. The experimental $^3P{:}^1D$ yield ratio for the second harmonics only is 1.1 while the theoretical ratio is 1.37. In comparison, this ratio is 2.0 for the weak ω, strong 2ω case.

6.3. Analysis: weak fundamental intensity, strong second harmonic intensity

For two-colour data, we note that experimental limitations may reduce the size of interference effects, compared to the theoretical values. The intensity ratio between the two colours may be not exactly as estimated. Furthermore, the degree of coherence is high but not perfect, or there may be small misalignments of the focal spots of the two wavelengths; all of these factors will affect the amplitude of the oscillations as a function of phase, by contributing a background that is not phase sensitive.

Table 1 shows that the theory predicts qualitatively the observations. The amplitude of oscillation (k) of the ^1D state is predicted well while k of the ^3P state is overestimated by a factor of nearly two. The theoretical overestimation of ^3P relative to ^1D may be due to the same reason discussed in the previous subsection. The interference channels we expect here are the one between the spLEAD (process (d) in figure 1) followed by process (b) and the direct ionisation (process (h)); both are from the initial state $2s^22p^5$. The relatively small numbers of k for both stems from the unbalanced amplitude ratio of these two channels; the spLEAD process (d) followed by (b) via weak ω two-photon absorption is much weaker than the direct process (h) via strong 2ω one-photon absorption.

The branching ratio $^3P{:}^1D$ is within 30% of the theoretical value. The theory predicts a phase lag between the oscillations of the ^3P and ^1D states of -0.38 rad, in agreement with the experimental value within the error.

In the previous study by Iablonskyi *et al* [4], weak oscillations of the ^3P peak were visible, comparable with the noise level, and it was concluded that the peak did not oscillate. We have reanalysed this data and find that the ratio of oscillation amplitude of the $^3P{:}^1D$ states is 0.15 ± 0.1, compared to the present value of 0.47 ± 0.2. The

difference is a little more than the statistical errors, and suggests systematic errors. Very recently, it has emerged that the transmission of the optical lens used in the VMI has non-uniform transmission (vignetting), resulting in fading sensitivity at the edges. This may have affected the results in the previous study.

6.4. Analysis: strong fundamental intensity, weak second harmonic intensity

In this case, based on the discussion in the previous subsection, one may expect relatively large values of k. Indeed, if we take account of only the interference between the spLEAD process (d) followed by (b) via strong ω two-photon absorption and the direct process (h) via weak 2ω one-photon absorption, the expected k values are more than 0.2 for both ^1D and ^3P. The measured k values are, however, 0.0085 and 0.01 for ^1D and ^3P, respectively. The reason for suppression of the interference is that another interference channel that was negligible for weak ω + strong 2ω becomes significant for strong ω + weak 2ω. This new interference channel is between the spLEAD channel (d) via strong ω and the direct ionisation (h) via weak 2ω following the stimulated emission (b) by strong ω. Here, the initial state of these two interfering channels is $2s2p^6$. This interference results in an oscillation amplitude of only 0.04 and 0.06 for ^1D and ^3P with almost opposite phase with respect to the other interference channel characterised by the $2s^22p^5$ initial state. According to the TD–ADC(1) simulation, under the condition of strong ω + weak 2ω, during the interaction of neutral Ne with the ionising pulses the time-averaged populations of the $2s2p^6$ excited state of Ne^+ is approximately the same as that of the $2s^22p^5$ ionic ground-state. Moreover, the two $2s2p^6$ and $2s^22p^5$ states of Ne^+ are incoherently populated, reflecting the maximum entanglement between the emitted photoelectron and the Ne^+ parent-ion system. Therefore, the experimentally observed yields and asymmetries can be described as the incoherent sum of those resulting from each of the two individual channels separately. Adding incoherently the two interference oscillations represented by $S^{2p}_{(i)}$ and $S^{2s}_{(i)}$:

$$A = \frac{S^{2p}_1 - S^{2p}_2 + S^{2s}_1 - S^{2s}_2}{S^{2p}_1 + S^{2p}_2 + S^{2s}_1 + S^{2s}_2}, \tag{10}$$

where $i = 1, 2$ and $2p$ and $2s$ represent the initial hole states for the two interference channels respectively, we obtain the results given in table 1; $k = 0.01$ for ^1D and $k = 0.032$ for ^3P. The theory once again predicts with very good accuracy the amplitude of oscillation for the ^1D final dication state, while the ^3P final state's calculated oscillation amplitude is overestimated, approximately by a factor of 3, with respect to the extrapolated experimental value. Accordingly, both the ratio of amplitudes and the ^3P:^1D branching ratio are overestimated by a factor of about 3. The reasons for the overestimation may be the same as those discussed in the previous two subsections. Once again, a phase lag is predicted, but with a value 0.74 less than the experimental value.

7. Conclusions

We have studied experimentally and theoretically the spLEAD of Ne, using four different experimental conditions: strong fundamental or second harmonic wavelength; strong second harmonic and weak second harmonic wavelength; weak second harmonic and strong fundamental wavelength. By scanning the phase between the two wavelengths, we observed interference effects in the PAD, which can only occur when the spLEAD channel is active. The theory predicts all phenomena observed, reproducing qualitatively the branching ratios of ^3P to ^1D final states as well as the ratios of oscillation amplitudes and phase lags. Reasons for the discrepancies at the quantitative level, where present, have been discussed. Since the phenomenon of spLEAD can only occur for correlated states, this study highlights the importance of configuration mixing in photoionisation. The physics and the technique are generally applicable, and in the future we plan to extend our studies to molecular systems, where the spLEAD process may be of significant importance.

Acknowledgments

Appendix

A.1. Ratio of Intensity of ω to 2ω

Processes (a) and (e) in section 2 lead to the emission of photoelectrons with kinetic energy $\sim$5 eV, while electrons emitted by process (g) have an energy $\sim$32 eV. The $2p$ cross sections for $\omega = 26.85$ eV and $2\omega = 53.7$ eV are $\sigma_1 = 8.4$ Mb and $\sigma_3 = 6.8$ Mb, while the $2s$ cross section at 53.7 eV is $\sigma_2 = 0.3$ Mb [22]. We obtain the following equation for the ratio of intensities of 5 and 32 eV electrons:

$$R_{5,32} = \left(\frac{I_\omega t_1 \sigma_1}{\omega} + \frac{I_{2\omega} t_2 \sigma_2}{2\omega} \right) \bigg/ \left(\frac{I_{2\omega} t_2 \sigma_3}{2\omega} \right), \tag{11}$$

where I_ω and $I_{2\omega}$ are the average intensities over the length of the pulse, and $t_1 = 40$ fs, $t_2 = 30$ fs are the pulse durations of the fundamental and second harmonic.

ORCID iDs

Lénárd Gulyás Oldal ⓘ https://orcid.org/0000-0003-2852-9945
Carlo Callegari ⓘ https://orcid.org/0000-0001-5491-7752
Giuseppe Penco ⓘ https://orcid.org/0000-0002-4900-6513
Kevin C Prince ⓘ https://orcid.org/0000-0002-5416-7354

References

[1] Meitner L 1922 *Z. Phys.* **9** 131–44
[2] Auger P 1923 *C. R. Hebd. Séances Acad. Sci.* **177** 169–71
[3] Cooper B and Averbukh V 2016 *Phys. Rev. Lett.* **111** 083004
[4] Iablonskyi D *et al* 2017 *Phys. Rev. Lett.* **119** 073203
[5] Ranitovic P, Tong X, Hogle C, Zhou X, Liu Y, Toshima N, Murnane M and Kapteyn H C 2011 *Phys. Rev. Lett.* **106** 053002
[6] Tong X M, Ranitovic P, Hogle C W, Murnane M M, Kapteyn H C and Toshima N 2011 *Phys. Rev. A* **84** 013405
[7] Avaldi L, Dawber G, Gulley N, Rojas H, King G C, Hall R, Stuhec M and Zitnik M 1997 *J. Phys. B: At. Mol. Opt.* **30** 5197–212
[8] Lyamayev V *et al* 2013 *J. Phys. B: At. Mol. Opt. Phys.* **46** 164007
[9] Allaria E *et al* 2012 *Nat. Photon.* **6** 699–704
[10] Dribinski V, Ossadtchi A, Mandelshtam V A and Reisler H 2002 *Rev. Sci. Instrum.* **73** 2634–42
[11] Prince K C *et al* 2016 *Nat. Photon.* **10** 176–9
[12] Svetina C, Cocco D, Mahne N, Raimondi L, Ferrari E and Zangrando M 2013 *J. Synchrotron Radiat.* **23** 35–42
[13] Svetina C *et al* 2015 *J. Synchrotron Radiat.* **22** 538–43
[14] Ruberti M, Averbukh V and Decleva P 2014 *J. Chem. Phys.* **141** 164126
[15] Simpson E R *et al* 2016 *New J. Phys.* **18** 083032
[16] Ruberti M, Decleva P and Averbukh V 2018 *Phys. Chem. Chem. Phys.* **20** 8311–25
[17] Ruberti M, Decleva P and Averbukh V 2018 *J. Chem. Theory Comput.* **14** 4991–5000
[18] Ruberti M 2019 *J. Chem. Theory Comput.* **15** 3635–53
[19] Ruberti M 2019 *Phys. Chem. Chem. Phys.* **21** 17584–604
[20] Bachau H, Cormier E, Decleva P, Hansen J E and Martin F 2001 *Rep. Prog. Phys.* **64** 1815–942
[21] Kramida A, Yu R, Reader J and (NIST ASD Team) 2015 NIST Atomic SpectraDatabase (ver. 5.3) http://physics.nist.gov/asd [11 March 2017] National Institute of Standards and Technology, Gaithersburg, MD
[22] Bizau J M and Wuilleumier F J 1995 *J. Electron Spectrosc. Relat. Phenom.* **71** 205–24